Characterization of nanoparticles through medium-energy ion scattering

M. A. Sortica, P. L. Grande, G. Machado, and L. Miotti
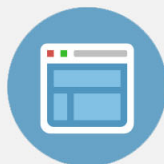
Characterization of nanoparticles through medium-energy ion scattering

M. A. Sortica,[1] P. L. Grande,[1,a)] G. Machado,[2,3] and L. Miotti[1,4]

[1]*Instituto de Física, Universidade Federal do Rio Grande do Sul, Avenida Bento Gonçalves 9500, 91501-970 Porto Alegre, Rio Grande do Sul, Brazil*
[2]*Centro de Ciências Exatas e Tecnologia, Universidade de Caxias do Sul, Rua Francisco Getúlio Vargas 1130, 95070-560 Caxias do Sul, Rio Grande do Sul, Brazil*
[3]*Centro de Tecnologias Estratégicas do Nordeste, Av. Prof°. Luiz Freire, 01. Cidade Universitária, CEP 50.740-540, Recife, Pernambuco, Brazil*
[4]*Department of Physics, North Carolina State University, Raleigh, North Carolina 27695-8202, USA*

In this work we review the use of the medium-energy ion scattering (MEIS) technique to characterize nanostructures at the surface of a substrate. We discuss here how the determination of shape and size distribution of the nanoparticles is influenced by the energy loss at the backscattering collision, which leads to an asymmetrical energy-loss line shape. We show that the use of a Gaussian line shape may lead to important misinterpretations of a MEIS spectrum for nanoparticles smaller than 5 nm. The results are compared to measurements of gold nanoparticles adsorbed on a multilayered film of weak polyelectrolyte. © *2009 American Institute of Physics.*
[doi:10.1063/1.3266139]

I. INTRODUCTION

Nanotechnology has brought some new challenges, not only for the development of new processes for synthesis of nanostructures but also for the characterization of them.[1] The latter is usually achieved by techniques involving incident electrons or photons (e.g., electron microscopy, x-ray spectroscopy and diffraction, and ultraviolet-visible spectroscopy), and to a less extent by using incident ions [e.g., Rutherford backscattering spectrometry (RBS)].[2]

Determining the depth distribution of different chemical elements near and at the surface of solids is of major importance for many aspects of nanotechnology. In principle, this can be accomplished quantitatively with deep subnanometric depth resolution, using ion scattering at energies corresponding to the maximum stopping power and high-energy resolution detection systems. The method is called medium-energy ion scattering (MEIS)[3–6] and uses typically 100–200 keV incident H^+ or He^+ ions, and combines the effects of elastic recoil energy loss and inelastic losses, as in a conventional Rutherford backscattering. The MEIS technique is widely used for analysis of microelectronic materials[4] as well as for the determination of structural and vibrational parameters of crystalline surfaces.[5] The former application exploits its high-energy resolution whereas the latter is achieved by measuring angular dips originated from shadowing and blocking effects.

More recently, the MEIS technique was used as an additional tool for characterization of Pt–Rh (Ref. 7) and Au nanoparticles[8,9] and of InAs–GaAs quantum dots.[10] Basically the nanoparticles' shape, composition, size distribution, and stoichiometry have been successfully obtained. In addition, the determination of the number of nanosize inhomogeneities in thin films was also investigated for some particular geo-

metrical shapes.[11] Nevertheless, the most promising MEIS application, namely, the determination of depth distributions of different elements in a single nanoparticle, still needs further investigations. This possible MEIS application is unique and is hardly achieved by any other analytical technique.[12]

In addition, the simple data analysis framework successfully used for other low-resolution backscattering techniques (such as RBS) is not applicable to MEIS, since the much higher energy resolution of MEIS reveals new spectral features.[13] The most relevant one is that in the first few angstroms below the solid surface the ion energy loss departs from a symmetric, Gaussian distribution. In fact, the departure from a Gaussian energy-loss distribution has been recently observed for near-surface collisions[14,15] and is very important to get reliable depth profiles of heavy elements in very thin films.[16] Thus, standard energy-loss theories or semiempirical methods based on Gaussian energy-loss distributions cannot be used for depth profiling in the subnanometric scale. Instead, an atomistic description of the electronic excitation process and its impact parameter dependence[13] has to be taken into account in a stochastic approach.[16,17] In particular, a direct experimental evidence of the influence of trajectory-dependent energy loss in scattering from the outermost few atomic layers of a single crystal, and corresponding modeling in a parameter-free fashion was recently proposed.[17] This approach is computationally very demanding, but recent works also show that a simple exponential modified Gaussian (EMG) (Ref. 18) can be used to describe asymmetrical energy losses found in MEIS experiments.[19] Indeed, the importance of the asymmetry of the energy loss in the characterization of nanoparticles is an important issue and was never investigated before, and as it will be shown in what follows, the use of Gaussian energy-loss distribution may lead to important misinterpretations of the MEIS spectrum.

a)Author to whom correspondence should be addressed. Electronic mail: grande@if.ufrgs.br.

In this work we developed a Monte Carlo simulation of MEIS spectra that considers any nanoparticle geometry and areal density, going beyond previous investigations that were restricted to few specific nanostructures' shapes and surface coverage.[7,20] Furthermore, the size distribution and areal density of the nanoparticles are also taken into account. The present method also includes the effect of the asymmetry of the energy-loss distribution due to a single violent collision such as the backscattering event. Using this method we investigated the influence of the nanoparticle geometry, areal density, size distribution, and energy-loss line shape on the one-dimensional (1D) (energy) and two-dimensional (2D) (energy and angle) MEIS spectra.

This paper is organized as follows. The crucial aspects of the MEIS technique are reviewed in Sec. II, while the simulation method of MEIS spectra is described in detail in Sec. III. The results of the simulations for different nanoparticles' geometries and areal densities are showed and discussed in Sec. IV. In particular, the effects of the asymmetry in the energy loss on the determination of nanoparticles' size distribution will be addressed. Finally, in Sec. V, the results of the present Monte Carlo simulations are compared to new measurements of gold nanoparticles grown on a surface of a polyelectrolyte [poly(allylamine hydrochloride) (PAH)].

II. MEIS TECHNIQUE

MEIS is based on the same principles of RBS;[21] however, the implementation and data analysis of MEIS are somehow different. A toroidal electrostatic energy analyzer, with a much larger solid angle, replaces the surface barrier detector used in the RBS analysis. The system presents a much better energy resolution, typically $\Delta E/E$ of about 10^{-3}; meanwhile both the energy and the scattering angle are simultaneously stored in a 2D multichannel system. Furthermore, as a consequence of the electrostatic nature of the analyzer, ions that are neutralized following interaction with the target are not deflected and thus ignored by the detection system. Therefore, quantitative measurements are constrained to light ions such as H and He, where the projectile charge-state fractions are relatively well known. In addition, the projectile energies have to be typically higher than 50 keV, where the scattering cross section is basically determined by the Rutherford formula, and the influence of the screening due to target and projectile electrons although important in some cases can be easily calculated. On the other hand the projectile energies should not exceed hundred of keV, as in the standard RBS, in order to keep the radius of the shadow cone by about the value of thermal vibrations. This enhances the sensitivity for first layers below the surface in the case of crystalline materials. For amorphous thin films, these energies are convenient because they are about the maximum of the electronic stopping power. For all these reasons the projectile energies are typically restricted to 50–200 keV.

As recently addressed,[18] the much higher energy resolution of MEIS reveals spectral features that cannot be resolved by solid-state detectors. The most relevant one is the asymmetry of the energy-loss distribution. Thus, the use of a symmetric, Gaussian distribution, well established for RBS analysis, becomes questionable. In principle there are many reasons for the asymmetry of the ion energy-loss distribution,[22] among them, two are important for the conditions found in MEIS experiments, namely, the stochastic nature of the energy-loss processes and the inelastic excitations and/or ionizations in a single nearly head-on collision such as the backscattering event. Both effects lead to a considerable asymmetry of the energy-loss distribution as long as the number of collisions is low, which holds true in the analysis of ultrathin films or small nanoparticles.

The experimental work was performed at the Ion Implantation Laboratory of the Physics Institute (Federal University of Rio Grande do Sul). A 500 kV electrostatic accelerator provided beams of H^+ at a nominal energy of 100 keV. The samples were mounted in a three-axis goniometer inside the analysis chamber kept under a pressure of about 10^{-7} mbar. Typical ion current was less than 15 nA and the samples were moved each 4.5 μC in order to avoid damage of the nanoparticles. In fact, we did not observe any significant changes in MEIS spectrum after a H irradiation of about 126 μC. A fraction of backscattered protons emerging from the target were analyzed in the toroidal electrostatic analyzer (TEA) mounted at 120° with respect to the beam direction. At the top end of the TEA a set of two microchannel plates coupled to a position-sensitive detector allows each ion to be energy and angle analyzed leading to 2D spectra. The TEA angular aperture is 30° and each angle bin corresponds to 0.08°. The overall energy resolution of the system is 350 eV. The details of the data analysis are found in Ref. 23. In short, the 2D spectrum has to be projected onto the energy axis for a particular set of angle bins in order to allow adequate processing of the information contained in them. This procedure of summing the energy spectra at different scattering angles (Θ) is performed correcting the variation of the kinematical factor $[K(\Theta)]$. However, the so-called path length correction associated with each angle bin, usually applied when analyzing thin films, cannot be performed when investigating nanoparticles, as it will become clear next.

III. SIMULATION PROCEDURE

General formulas to simulate MEIS or RBS spectra were proposed only for particular shapes of nanostructures such as for spherical and columnar nanoparticles (or inhomogeneities).[11] Here we followed a quite general approach, where any nanoparticle geometry, inclusions, porous, inhomogeneities, and their corresponding areal and size distributions are accounted for. To this end, we use the Monte Carlo method for the three-dimensional (3D)-spatial integrations and determine the incoming- and outgoing-projectile paths numerically from the incident and scattering angles. Nowadays, this approach is not computationally demanding anymore and the typical computing time to obtain a full 2D spectrum is about 10 min in a fast Pentium 3GHz.

The underlying physics to obtain the geometry of the nanoparticles and the corresponding areal density is the energy-loss spreading caused by the nanostructure, so called structure-induced energy spread. It was recently used to ana-

lyze the number and size of inhomogeneities in thin films (inclusions of spherical or columnar materials or voids) in Ref. 11.

As in Ref. 7, the nanoparticles are divided into small cells (with volume dV) and the yield of incident ions, detected with energy E, and backscattered by atoms of the ith element in the cell located at the jth position in a sample is given by

$$dH_{ij}(E) = x_i Q \Omega \sigma_i(E_1, \Theta) f(E - E_{out}) dE F^+(E) N_j dV, \quad (1)$$

with $E_1 = E_0 - \Delta E_{in}$ and $E_{out} = K_i(\Theta)E_1 - \Delta E_{out}$, where x_i is the atomic fraction of the ith element in the jth position, Q is the fluence of incident ions, Ω is the solid angle subtended by the detector, $\sigma_i(E_1, \Theta)$ is the differential scattering cross section for the ith element, N_j is the atomic density at the jth position, the energies E_0, E_1, and E_{out} are the incident energy, the energy just before the backscattering, and the detected energy, respectively, $K_i(\Theta)$ is the kinematical factor, ΔE_{in} and ΔE_{out} are the energy losses along the incoming and outgoing paths, respectively, $f(E - E_{out})$ is the energy-loss distribution, and $F^+(E)$ is the correction function due the neutralization probability of the ions.

The differential scattering cross section $\sigma_i(E_1, \Theta)$ is obtained here by solving the orbit equation using the Ziegler-Biersack-Littmark interatomic potential.[24] The neutralization probability correction $F^+(E)$ is determined from the Marion and Young data.[25] The energy-loss distribution $f(E - E_{out})$ is due to all energy-loss fluctuations arising from the interaction with target atoms and detection system. In the RBS technique, a Gaussian distribution has been used for $f(E - E_{out})$ because of the large number of inelastic interactions that cannot be resolved by the detection system of the technique. Here we use the EMG distribution for $f(E - E_{out})$,[18] which is a simple analytical formula obtained by the convolution of a Gaussian distribution with an exponential distribution that represents the inelastic energy loss due to ionization and excitation of the backscattering atom. The energy-loss distribution f reads

$$f(\Delta E) = \alpha \exp(-\alpha \Delta E) H_{step}(\Delta E)^* \frac{1}{\sigma\sqrt{2\pi}} \exp\left(-\frac{\Delta E^2}{2\sigma^2}\right)$$

$$= \alpha/2 \exp[-\alpha/2(2\Delta E - \sigma^2 \alpha)]$$

$$\times \{1 + erf[(\Delta E - \sigma^2 \alpha)/(\sigma\sqrt{2})]\}, \quad (2)$$

where $H_{step}(\Delta E)$ is the Heaviside step function, σ is the Gaussian straggling, and $\alpha^{-1} = \sigma_o$ is the standard deviation for the electronic energy-loss distribution in a single collision with impact parameter $b \sim 0$. The $f(\Delta E)$ distribution described by Eq. (2) can be shifted by $1/\alpha$ to set the mean energy loss to zero. In addition, for $\alpha\sigma \gg 1$, the EMG approaches to a Gaussian function. In fact, for $\alpha\sigma > 5$, the EMG can be replaced with a Gaussian function in order to avoid numerical problems.

The MEIS spectrum H(E) of the sample is obtained by integrating Eq. (1) for the entire sample and summing up for all elements. If the sample is a homogeneous film, for any given backscattering position, the incoming and outgoing paths depend only on the depth (as long as the incidence and

detected directions are fixed). Thus, the integration is performed along the depth only. In a nanostructured sample, this does not hold true and the full 3D integration is needed. For this purpose, the sample has to be built in a 3D matrix [corresponding to the j index from Eq. (1)] and the full 3D integration is performed through the Monte Carlo method. In this way, any geometrical shape on top of a surface or embedded in a host target can be considered. Other stochastic parameters are the energies and angles (for the 2D mode) of the detected projectiles. Furthermore the size and the shape of the nanoparticles can be chosen stochastically from any size and shape histograms. The present simulation algorithm can be summarized as follows.

(i)   The sample is composed by a collection of nanostructures, each of them having different geometries and sizes. Each geometry (g) and size (t) has a statistical weight p_g and p_t, respectively, and it is divided into many cubes of volume typically of 10^{-3} nm^3. Each cell (x,y,z) has elemental composition x_i, atomic density N_j, stopping power (dE/dx), and energy-loss straggling (dW^2/dx) determined from the input.

(ii)   The backscattering position (x,y,z), the nanoparticle geometry (g), and size (t) are generated by random numbers.

(iii) The incoming path is calculated as a straight line. Since the incident ion may penetrate more than one nanostructure along its inward path, depending on the projectile, the incidence angle θ_1, the areal density of nanoparticles is taken into account. The mean energy loss ΔE_{in} and the squared variance ΔW^2_{in} are calculated from the dE/dx and dW^2/dx, respectively, of each cell along the inward path.

(iv)   In the same way, the mean energy loss ΔE_{out} and squared variance ΔW^2_{out} are calculated for the outgoing path, given by the detection angle θ_2.

(v)   The energy-loss distribution from Eq. (2) is calculated, using the parameter σ^2 for the energy-loss straggling along the incoming and outgoing paths $K_i^2(\Theta)\Delta W^2_{in} + \Delta W^2_{out}$ and the asymmetry parameter α (or σ_0^{-1}) either from experiments[19] or from calculations.[18,26]

(vi)   For each ith element in the (x,y,z) composition, we calculate the yield through Eq. (1) weighted by p_g and p_t.

The final energy-loss spectrum associated with the emerging ions was then convoluted with the instrumental function for comparisons with the experimental data. Following the results of our earlier work on energy loss from single collisions, we have used a Gaussian function with squared σ_D^2 to describe the instrumental resolution. Thus, this value was simply added to σ^2 in Eq. (2). It is pointed out that the asymmetry of the scattered ion energy spectra arises entirely from the use of the EMG function and depth-dependent Bohr straggling. To validate the present Monte Carlo method we compared its results to previous ones of Konomi[7] and Kido[20] for the same input parameters and same energy-loss distribution function (Gaussian line shape), and no difference was observed.
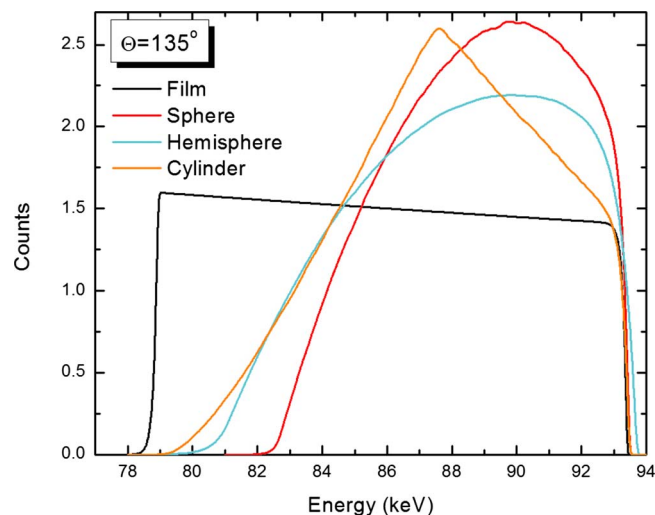
FIG. 1. (Color online) Simulated MEIS spectra for a reduced straggling value and improved energy resolution (see Table I), for different geometries of gold nanoparticles using incident 100 keV He$^+$ ions.
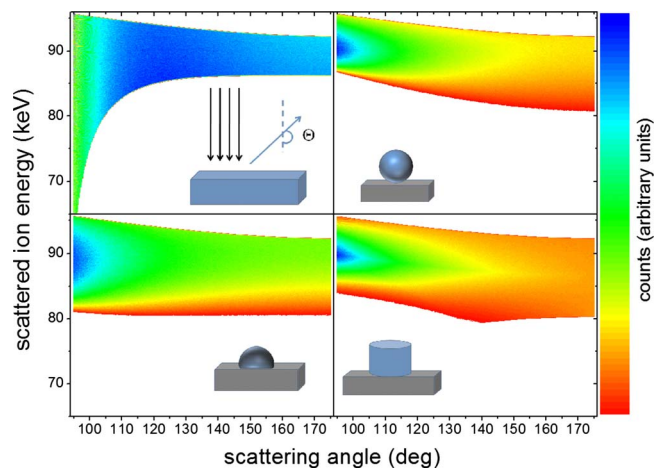

FIG. 2. (Color online) 2D map of scattered ion intensities as a function of scattering angle and scattered ion energy for incidence of 100 keV He$^+$ ions.

IV. RESULTS AND DISCUSSION

The results of the simulations for different geometrical shapes of gold nanoparticles are shown in Fig. 1 for 100 keV He$^+$ ions impinging at normal incidence and scattered at 135°. Four standard nanoparticle geometries were selected, namely, a film with thickness t=10 nm, a sphere with diameter=t, a hemisphere of radius r=t, and a cylinder with height h and radius r equal to t. The parameters used in the simulation, namely, atomic density, stopping power, straggling, asymmetry factor, and energy resolution, are shown in Table I. In the simulation of the spectra in Fig. 1, the energy-loss straggling and experimental Full Width at Half Maximum ($\Gamma_D = 2.35\sigma_D$) were artificially reduced in order to enhance the effect of structured-induced energy spread.

As can be observed in Fig. 1, the different path lengths of ions associated with each nanoparticle geometry result in very different MEIS spectra. In general, the spectra for nanoparticles have larger energy-loss variations in comparison to uniform films. These effects, also called structured-induced energy spread,[30] lead to an energy spectrum with a rounded maximum (no plateau is observed). Of course, these differences can be observed as long as the electronic energy-loss straggling is not too large. In this way, uncertainties in the energy-loss straggling parameters may prevent the correct determination of the nanoparticles' geometry.

TABLE I. Parameters of the simulations shown in each figure of this work. The values for the stopping power, straggling, and σ_o were extracted from the SRIM 2008 tables (Refs. 24 and 27) Chu formula (Ref. 28), and CASP 4.0 (Ref. 29), respectively.

Figure	Projectile	Energy (keV)	ρ (g/cm^3)	dE/dx (eV/Å)	dW^2/dx (eV^2/Å)	σ_o (eV)	Γ_D (eV)
1–3	He$^+$	100	19.31	30.83	1[a]	179	80[a]
4, 5, 7, and 8	H$^+$	100	19.31	21.07	1850	257	400

[a]Reduced values were used in order to enhance the geometrical effects of the nanoparticles.

The best way to determine the shape of a nanoparticle through the MEIS technique is to look at all different scattering angles available since each geometrical shape has a typical angular dependence of the backscattering yield. For normal incidence, Fig. 2 shows this angular dependence for the four geometries and beam parameters mentioned above. The overall features are the following. As well known, for films, the decrease in the highest backscattering energy (the front edge in a 1D MEIS spectrum) with increasing scattering angle is only due to the variation of the kinematical factor K(Θ). The rapid decrease in the lowest detected energy for smaller scattering angles is a direct consequence of the enhanced path length [by the factor $1/\cos(\theta)$] in a grazing detection direction. Thus, the energy-loss spectrum is much wider at smaller scattering angles. In the case of a spherical nanoparticle, as depicted in Fig. 2, we have the opposite. In normal incidence, the maximum path length of two diameters is found at the scattering angle of 180°, which makes the energy loss wider at large scattering angles. For the hemisphere (see Fig. 2), the enhancement of the path length at larger scattering is not as important as in a sphere, neither the enhancement at smaller scattering angle is as large as in a film. In this way, the lowest energy edge will depend weakly on the scattering angle. Finally, the cylindrical geometry (representing disks, wires, or columnar structures) is peculiar because the energy spectrum is widest at an intermediate scattering angle, where the outgoing particles can travel along a major diagonal of the cylinder. Thus, MEIS could easily identify uniformly right or oblique cylinders.

The situation changes when the ions can interact with two or more nanoparticles along their incidence or detecting directions. Therefore, the areal density of nanoparticles has to be considered. Figure 3 shows the spectra for the same nanoparticles' geometries as Fig. 2, but with the maximal possible areal density (nanoparticles touching each other). At this high areal density of nanoparticles the projectile may go through many nanoparticles and the final energy-angle spectra will look very similar to the one for a rough film. The strong modulation in the energy of the low-energy edge of the contour map is a direct manifestation of this.
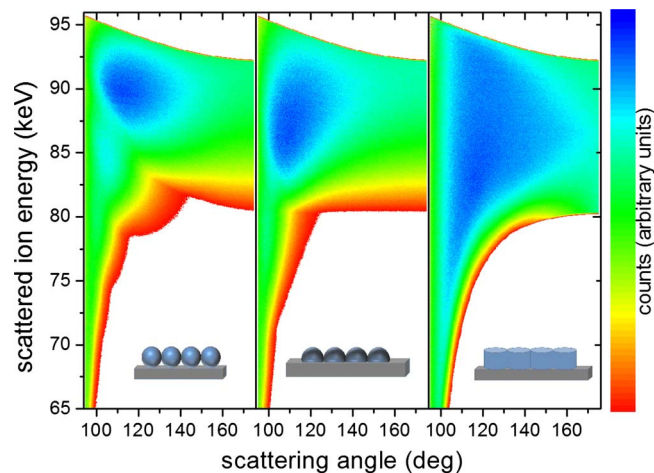
FIG. 3. (Color online) The same as in Fig. 2, but for the maximum areal density of nanoparticles.

The influence of the energy-loss asymmetry due the backscattering collision is shown in Fig. 4 in the case of spherical gold nanoparticles with different diameters and 100 keV of H^+ scattered at 135°. The parameters of the simulations can be found in Table I. The dashed lines represent the simulations using the standard Gaussian line shape whereas the solid lines correspond to simulations using asymmetrical line shape (EMG). Figure 4 shows that for small nanoparticles (diameter less than 5 nm) the simulations using different line shapes are significantly distinct, in a similar way as recently observed for thin films[16] where the negligence of the line shape asymmetry can result in a misinterpreted diffusion process of a thin film into its substrate. In the case of nanoparticles, other misinterpretations could also happen, such as a wrong shape, areal density, or size distribution of the nanoparticles. For example, for MEIS spectra of Au nanoparticles, recently measured,[20] the authors claimed that a disk-shaped nanoparticle geometry could be immediately ruled out, since the energy spectrum of such thin disks differs from nanospheres considerably. Neverthe-
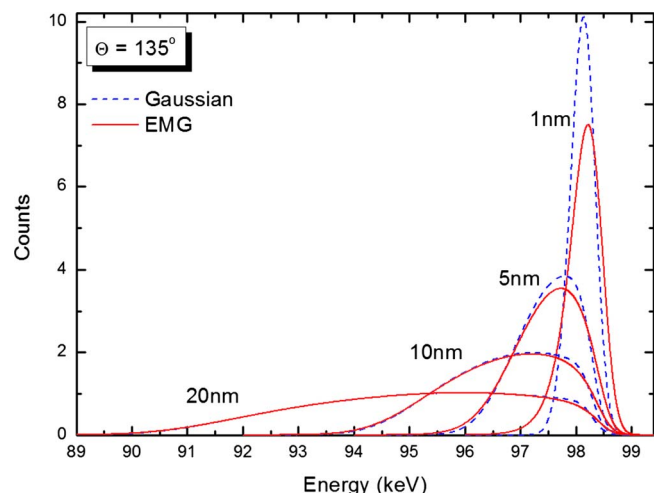

FIG. 4. (Color online) Comparison between simulated spectra with Gaussian and EMG energy-loss distributions for different diameters of spherical Au nanoparticles using realistic values for energy straggling and resolution for 100 keV H^+ ions.
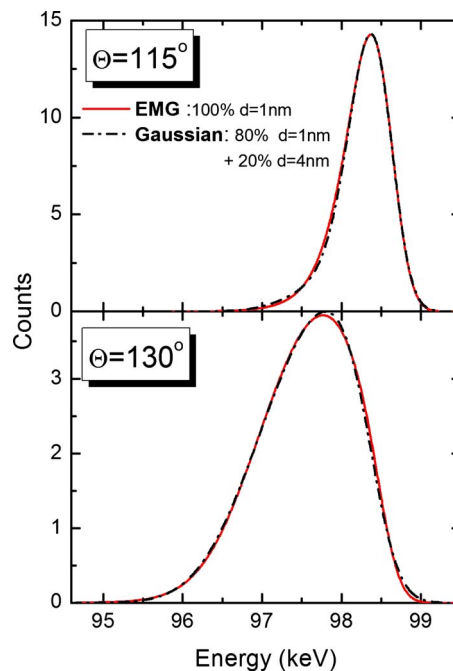

FIG. 5. (Color online) Simulated MEIS spectra using (solid lines) EMG line shape for spherical Au nanoparticles of well defined diameter of 1 nm, and (dashed lines) Gaussian line Au nanoparticles with size distribution indicated in the legend. The spectra are alike even at different scattering angles.

less, they used a Gaussian line shape for the corresponding MEIS simulations. If the actual asymmetry is taken into account, both geometries will have very similar MEIS spectra and the decision in favor of the spherical shape is achieved only by comparing the spectra at different scattering angles.[31] As a matter of fact, misinterpretations of the geometrical shape and/or areal density of nanoparticles due to neglecting the asymmetry of the line shape are not really an issue as long as the MEIS spectra are considered at different scattering angles.

Although different scattering angles can help to determine the nanoparticle geometry, the size distribution of the nanoparticles could be easily misinterpreted if the proper line shape is not accounted for. Figure 5 depicts this issue comparing the simulated MEIS spectra using the Gaussian or the EMG line shape at scattering angles of 115° and 130°. One can observe that the simulation using the EMG line shape for spherical nanoparticles with diameter d=1 nm is very similar to the simulation based on a Gaussian line shape but with a nanoparticle size distribution of 80% with d=1 nm and 20% with d=4 nm. In other words, in the case of small nanoparticles, a false size distribution of the particles can emulate the effect of the actual asymmetrical energy-loss line shape providing nearly the same angular dependence.

V. COMPARISON WITH EXPERIMENTAL DATA

A sample containing Au nanoparticles was prepared using the layer-by-layer (L-b-L) process to get nanoparticles with specific size through methodology.[32,33] Here, the polyelectrolyte multilayer was used to bind nanoparticles. This process involves deposition of weak polyelectrolytes from diluted aqueous solution, based on electrostatic interactions
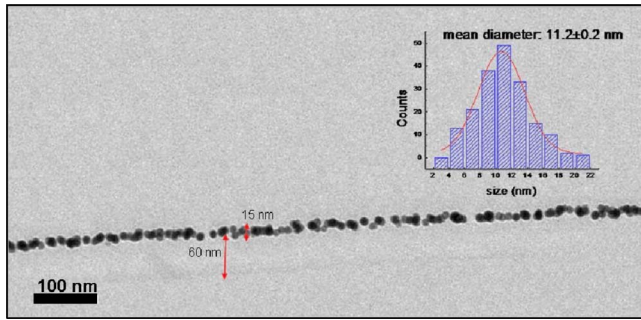
FIG. 6. (Color online) TEM image and size distribution of gold nanoparticles (inset).
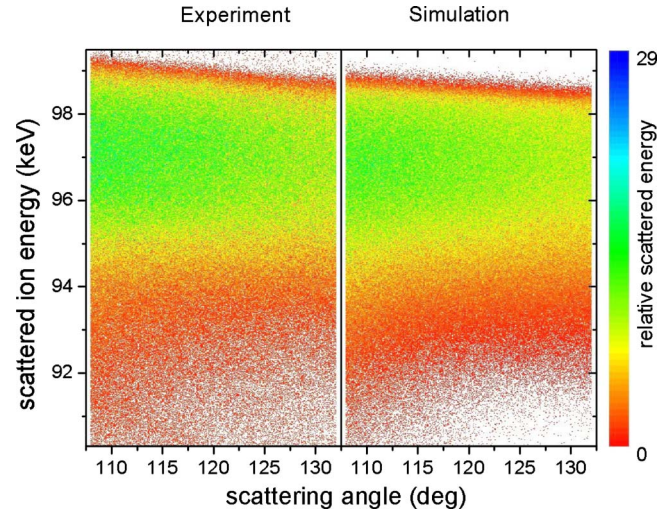

FIG. 7. (Color online) 2D map of scattered ion intensities as a function of scattering angle and scattered ion energy for incidence of 100 keV H ions. The experimental data are shown on the left and the theoretical simulation on the right.

of opposite polymer charges and specific substrates. A silicon wafer was immersed in an aqueous solution with polycation of PAH (Mw=70 000; Sigma-Aldrich) for 15 min and then withdrawn from the solution and rinsed in de-ionized water. The substrate was then immersed in a 25% aqueous solution of poly(acrylic acid) (PAA) used as polyanion (Mw =90 000; Polysciences) for 15 min and then rinsed in de-ionized water. The polyelectrolytes were used as received without further purification and were prepared as $1 \times 10^{-2}M$ solutions (based on the repeat-unit molecular weight) in ultrapure 18 MΩ cm de-ionized water (Millipore Milli-Q). The films were prepared for (PAH7.5/PAA3.5)10, where 3.5 and 7.5 correspond to the polyelectrolyte solution pH and 10 is the number of bilayers.

Gold nanoparticles were synthesized using the classic citrate method.[34] This method produces monodisperse gold nanoparticles with size distribution between 15 and 20 nm. Briefly, an aqueous solution of hydrogen tetrachloroauric acid (lll) hydrate (HAuCl$_{4.3}$H$_2$O; Strem chemicals, 99.9%) was reduced by sodium citrate dihydrate (Strem chemicals, 99%) in aqueous solution. A stock gold solution was prepared by dissolving 0.17 g of HAuCl$_4$ in 100 ml of water. 1 ml of stock gold solution was added to 18 ml of water and was then heated until it gets boiled. To this solution was added 1 ml of 0.5% sodium citrate solution, as soon as boiling commenced, causing the mixture to change from pale purple to a cherry red color. After obtaining the cherry red color the solution was boiled for an additional 10 min and then it was cooled slowly to room temperature. The PAH/PAA multilayer films were immersed into a gold aqueous solution (pH6.0) for 1 h and then removed and rinsed in de-ionized water for 1 min three times.

The samples were first characterized by transmission electronic microscopy (TEM) using JEOL 200CX operated at 120 kV. The Au nanoparticles' image and the inset for the corresponding size distribution are found in Fig. 6. The gold nanoparticles obtained are spheres with mean diameter of about 11.2 nm.

The experimental and simulated MEIS energy-angle spectra for the gold nanoparticles described above are shown in Fig. 7. The simulation was performed considering spherical Au nanoparticles separated from each other by 8 nm, and the best fit criterion was the minimum chi squared for three different scattering angles. The agreement is very good and the remaining differences can be attributed to a better de-

scription of the target. In fact, overlapping nanoparticles and their distribution in depth and distance from each other were not included in the simulation. Overlapping nanoparticles are visible in the TEM cross-view image, but they are the result of projection on the transversal plane. If we have considered any other geometry, the resulting 2D spectra would be significantly different from the experimental one. Concerning the determination of size distribution of nanoparticles, the uncertainties are about 5% for the mean diameter and 15% for the standard deviation. For the present case of nanoparticles with mean diameter of about 11 nm, the use of the Gaussian energy-loss distribution would affect the prediction of the mean diameter by only 3%. The comparison of the full energy-angle distributions is a unique feature of the present simulation method.

Figure 8 shows experimental 1D spectra for three selected scattering angles and compares them to simulated MEIS spectra for gold spherical nanoparticles and for a homogeneous thin film. As discussed in Sec. IV, the input parameters for an incorrect geometry, a film in this example, can be selected to best fit the experimental data for a given scattering angle, but it is not possible to find a single set of input parameters that allows for a good fitting for different scattering angles.

VI. CONCLUSIONS

The main results of the present investigation can be summarized as follows.

(a) We observed that, although the influence of the energy-loss distribution on the MEIS spectrum is significant only for small nanoparticles (diameter<5 nm), the use of the actual nanoparticle geometry is important for all sizes of nanostructures.

(b) Neglecting the asymmetry of the energy loss leads to a false nanoparticle size distribution in the case of small nanoparticles.
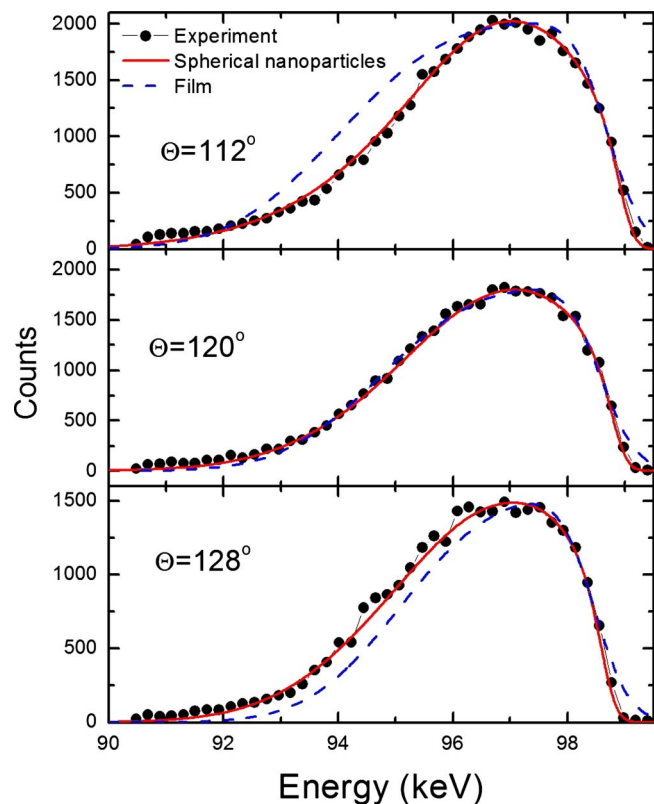
FIG. 8. (Color online) Fitting of experimental MEIS spectrum for spherical gold nanoparticles, assuming spherical nanoparticles and film. The best fit obtained for the nanoparticles at 120° for scattering angle (top) agrees with TEM characterization, while the best fit for a film needs unrealistic straggling values.

(c)   The method used here is the first to our knowledge not restricted to a few nanoparticles' shapes and surface coverage.

Finally, we used the method described here to simulate MEIS spectra and determine the shape and size distribution of gold nanoparticles adsorbed on a multilayered film of weak polyelectrolyte. The parameters obtained for the nanoparticles from the simulation of experimental MEIS spectra agree quite well with an image obtained by TEM of the sample. Furthermore, the corresponding MEIS spectra cannot be fitted by any other geometry as long as the angular dependence is considered.

ACKNOWLEDGMENTS

[1]J.-H. Kim, W. W. Bryan, H.-W. Chung, C. Y. Park, A. J. Jacobson, and T. Randall Lee, ACS Appl. Mater. Interfaces **2009**, 1063 (2009).
[2]S. J. Rosenthal, J. McBride, S. J. Pennycook, and L. C. Feldman, Surf. Sci. Rep. **62**, 111 (2007).
[3]J. F. van der Veen, Surf. Sci. Rep. **5**, 199 (1985).
[4]R. C. M. de Almeida and I. J. R. Baumvol, Surf. Sci. Rep. **49**, 1 (2003); M. Copel, IBM J. Res. Dev. **44**, 571 (2000); J. M. J. Lopes, U. Littmark, M. Roeckerath, E. Durgun-Ozben, U. Breuer, A. Besmehn, A. Stärk, P. L. Grande, M. A. Sortica, C. Radtke, J. Schubert, and S. Mantl, Appl. Phys. A: Mater. Sci. Process. **96**, 447 (2009).
[5]D. P. Woodruff, D. Brown, P. D. Quinn, T. C. P. Noakes, and P. Bailey, Nucl. Instrum. Methods Phys. Res. B **183**, 128 (2001).
[6]D. P. Woodruff and T. A. Delchar, *Modern Techniques of Surface Science*, 2nd ed. (Cambridge University Press, Cambridge, 1994).
[7]I. Konomi, S. Hyodo, and T. Motohiro, J. Catal. **192**, 11 (2000).
[8]T. Okazawa, M. Fujiwara, T. Nishimura, T. Akita, M. Kohyama, and Y. Kido, Surf. Sci. **600**, 1331 (2006).
[9]T. Okazawa, M. Kohyama, and Y. Kido, Surf. Sci. **600**, 4430 (2006).
[10]P. D. Quinn, N. R. Wilson, S. A. Hatfiled, C. F. McConville, G. R. Bell, T. C. Q. Noakes, P. Bailey, S. Al-Harthi, and F. Gard, Appl. Phys. Lett. **87**, 153110 (2005).
[11]J. P. Stoquert and T. Szörényi, Phys. Rev. B **66**, 144108 (2002).
[12]S. Horiuchi, S. Horie, and K. Ichimura, ACS Appl. Mater. Interfaces **1**, 977 (2009).
[13]P. L. Grande, A. Hentz, G. Schiwietz, W. H. Schulte, B. W. Busch, D. Starodub, and T. Gustafsson, Phys. Rev. B **69**, 104112 (2004).
[14]S. K. Srivastava, D. Plachke, A. Szokefalvi-Nagy, J. Mayor, and H. D. Carstanjen, Nucl. Instrum. Methods Phys. Res. B **219–220**, 364 (2004).
[15]A. Hentz, G. S. Parkinson, A. J. Window, P. D. Quinn, D. P. Woodruff, P. L. Grande, G. Schiwietz, P. Bailey, and T. C. Q. Noakes, Phys. Rev. B **74**, 125408 (2006).
[16]R. P. Pezzi, P. L. Grande, M. Copel, G. Schiwietz, C. Krug, and I. J. R. Baumvol, Surf. Sci. **601**, 5559 (2007).
[17]A. Hentz, G. S. Parkinson, P. D. Quinn, M. A. Munoz-Marquez, D. P. Woodruff, P. L. Grande, G. Schiwietz, P. Bailey, and T. C. Q. Noakes, Phys. Rev. Lett. **102**, 096103 (2009).
[18]P. L. Grande, A. Hentz, R. P. Pezzi, I. J. R. Baumvol, and G. Schiwietz, Nucl. Instrum. Methods Phys. Res. B **256**, 92 (2007); K. Dan. Vidensk. Selsk. Mat. Fys. Medd. **52**, 151 (2006).
[19]M. Hazama, Y. Ktisudo, T. Nishimura, Y. Hoshino, P. L. Grande, G. Schiwietz, and Y. Kido, Phys. Rev. B **78**, 193402 (2008).
[20]A. Iwamoto, T. Okazawa, T. Akita, I. Vickridge, and Y. Kido, Nucl. Instrum. Methods Phys. Res. B **266**, 965 (2008).
[21]W. K. Chu, J. W. Mayer, and M.-A. Nicolet, *Backscattering Spectroscopy* (Academic, New York, 1978).
[22]P. Sigmund, *Particle Penetration and Radiation Effects: General Aspects and Stopping of Swift Point Charges* (Springer, New York, 2006).
[23]S. M. Shubeita, M. A. Sortica, P. L. Grande, and J. F. Dias, Phys. Rev. B **77**, 115327 (2008).
[24]J. F. Ziegler, J. P. Biersack, and U. Littmark, *The Stopping Power and Range of Ions in Solids* (Pergamon, New York, 1985).
[25]J. B. Marion and F. C. Young, *Nuclear Reaction Analysis—Graphs and Tables* (North-Holland, Amsterdam, 1968).
[26]R. P. Pezzi, C. Krug, P. L. Grande, E. B. O. da Rosa, G. Schiwietz, and I. J. R. Baumvol, Appl. Phys. Lett. **92**, 164102 (2008).
[27]J. Ziegler, SRIM—The stopping and ranges of ions in matter, http://www.srim.org/.
[28]W. K. Chu, Phys. Rev. A **13**, 2057 (1976).
[29]P. L. Grande and G. Schiwietz, CASP 4.0—Convolution approximation of swift particles, http://www.helmholtz-berlin.de/people/gregor-schiwietz/casp_en.html.
[30]E. Szilágyi, Nucl. Instrum. Methods Phys. Res. B **183**, 25 (2001); E. Szilágyi, F. Paszti, and G. Amsel, *ibid.* **100**, 103 (1995).
[31]Y. Kido, personal communication (27 Nov. 2008).
[32]N. A. Kotov, I. D. Ckiiny, and J. H. Fendler, J. Phys. Chem. **99**, 13065 (1995).
[33]J. F. Ciebien, R. E. Cohen, and A. Duran, Supramol. Sci. **5**, 31 (1998).
[34]J. Turkevich, P. L. Stvenson, and J. Hillier, Discuss. Faraday Soc. **11**, 55 (1951).